Programming DNA Tube Circumferences

Peng Yin,[1,2,3]† Rizal F. Hariadi,[4] Sudheer Sahu,[6] Harry M. T. Choi,[2] Sung Ha Park,[1,5]* Thomas H. LaBean,[6,7] John H. Reif[6]

Synthesizing molecular tubes with monodisperse, programmable circumferences is an important goal shared by nanotechnology, materials science, and supermolecular chemistry. We program molecular tube circumferences by specifying the complementarity relationships between modular domains in a 42-base single-stranded DNA motif. Single-step annealing results in the self-assembly of long tubes displaying monodisperse circumferences of 4, 5, 6, 7, 8, 10, or 20 DNA helices.

DNA, life's information carrier, has recently emerged as a versatile material for constructing self-assembled synthetic molecular structures and devices (*1*–*4*). The construction of extended DNA arrays has motivated the search for rigid molecular building blocks, as component rigidity is commonly considered necessary for the formation of well-ordered DNA crystals rather than ill-defined aggregates (*5*). A typical building block, or tile, has a rigid structural core and displays several "sticky ends" that allow for specific binding with other tiles to guide lattice formation (*6*, *7*). Diverse tiling lattices have been constructed (*8*), and some of these lattices are reported to form tubes (*9*–*15*). Such DNA nanotubes typically have varied circumferences.

As the precise control of the structure of matter is a central goal for nanotechnology, materials science, and supermolecular chemistry, controlling DNA tube circumferences has attracted intense research interest. One strategy is to encode the circumferential tube geometry directly in each individual building block (*16*–*21*): barrel-like and/or half-barrel–like rigid tiles with designed tubular curvature and circumference are first assembled and then stacked to produce tubes with prescribed circumferences. Using this strategy, researchers have successfully constructed DNA tubes containing three (*17*, *18*), six (*16*, *20*, *21*), and eight circumferential helices (*21*) and have proposed designs for tubes of arbitrary circumference (*19*). However, this approach requires the circumference-dependent construction of distinct building blocks that often have complicated molecular structures. This motivates us to search for alternative strategies that are modular and simpler.

We report the construction of DNA lattices using a flexible, single-stranded DNA motif, which is substantially simpler than the current practice of using multistranded rigid tiles. During lattice formation, the motif configures itself into a tilelike geometry, and motif-motif interactions result in emergent rigidity along the extended growth direction of the lattice. Importantly, this flexible motif allows us to program the tube circumference also as an emergent property collectively defined by the modular interactions between the motifs. In the resulting framework, simply pairing modular domains in the single motif results in the self-assembly of monodisperse DNA tubes with designed circumferences. Additionally, the motif-based, codified construction permits the description of a tube design in the form of an abstract "molecular program," further simplifying the design process.

The 42-nucleotide (nt) single-stranded DNA motif has four concatenated modular domains (Fig. 1A): The orange domain 1 and the blue domain 2 together contain 21 nucleotides; the green domain 3 and the pink domain 4 together contain 21 nucleotides. By pairing up complementary domains, the motifs can be arranged to form DNA lattices composed of parallel DNA helices connected by single-stranded linkages [or half-crossovers (*22*)] (Fig. 1B). As the orange-blue domains and the green-pink domains in a motif each measure 21 nt, the interhelix linkages are spaced periodically at every two full helical turns (i.e., 21 base pairs). In the lattices, each nonboundary motif is configured into a rectangle-like shape and is connected to four adjacent neighbors. Thus the motif implements the functionality of a tile and is termed a single-stranded tile, or SST (see fig. S1 for the comparison between a traditional rigid multistranded tile and SST). In Fig. 1B, the number k associated with a green domain indicates the number of nucleotides contained in the domain and determines the putative, approximate interhelix curvature for an unstrained lattice (e.g., not closed into tubes) through a simple formula, $k \times 34.3° - 330°$ [see supporting online material (SOM) text S1 for details].

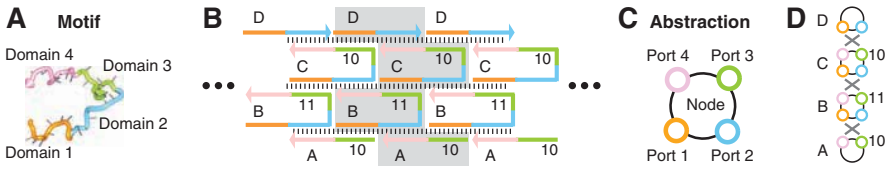

Fig. 1. (**A**) Motif. Colored lines represent modular domains; the arrowhead indicates the 3′ end. (**B**) Secondary structure of DNA lattices. Short vertical bars represent base-pairing. The shaded area indicates a repeating structural unit. (**C**) Abstraction of the motif as a node with four ports (*24*). The ports are depicted as colored circles. The color use is consistent with that in (A), and the ordering of the ports is specified by their colors: orange → blue → green → pink. (**D**) Complementarity graph.

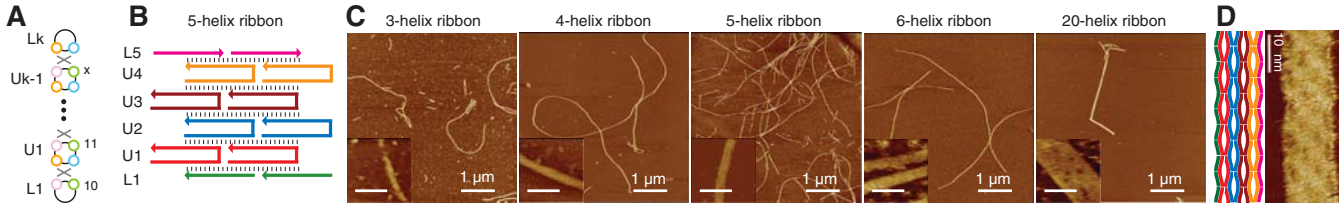

Fig. 2. Monodisperse DNA ribbons with programmed widths. (**A**) The molecular program for assembling a k-helix ribbon. (**B**) Secondary structure for the five-helix ribbon. See figs. S3 and S4 for more structures and details. (**C**) AFM images of 3-, 4-, 5-, 6-, and 20-helix ribbons. See fig. S5 for larger AFM images. (Insets) Scale bar, 50 nm. Measured ribbon widths: 9.3 ± 0.6 nm (3-helix ribbon), 12.4 ± 0.4 nm (4-helix), 15.0 ± 0.5 nm (5-helix), 18.1 ± 0.8 nm (6-helix), and 59.4 ± 1.3 nm (20-helix). See fig. S6 for ribbon width measurements. (**D**) High-resolution AFM image of the five-helix ribbon. (Left) Depiction of the expected DNA structure, emphasizing bended helices and interhelix gaps. The color use is consistent with (B). (Right) AFM image revealing an alternating pattern of four columns of interhelix gaps, in agreement with the depiction on the left. See fig. S7 for details.

[1]Department of Computer Science, California Institute of Technology, Pasadena, CA 91125, USA. [2]Department of Bioengineering, California Institute of Technology, Pasadena, CA 91125, USA. [3]Center for Biological Circuit Design, California Institute of Technology, Pasadena, CA 91125, USA. [4]Department of Applied Physics, California Institute of Technology, Pasadena, CA 91125, USA. [5]Center for the Physics of Information, California Institute of Technology, Pasadena, CA 91125, USA. [6]Department of Computer Science, Duke University, Durham, NC 27708, USA. [7]Department of Chemistry, Duke University, Durham, NC 27708, USA.

*Present address: Department of Physics, SKKU Advanced Institute of Nanotechnology, Sungkyunkwan University, Suwon, 440-746, Korea.

†To whom correspondence should be addressed. E-mail: py@caltech.edu

Downloaded from www.sciencemag.org on August 7, 2008

The modularity and standardization of the SST motif allow us to codify the lattice design procedure. First "wire" together complementary domains and then assign the dimensions of the green domains (*23*). The codification further permits us to ignore molecular structure details and express the lattice design in a simple abstract form. Adapting a previous notation system (*24*), we abstract our motif as a node with four ports, where each port represents a modular domain (Fig. 1C). The lattice design is expressed as a complementarity graph (Fig. 1D), where two complementary ports are connected by a gray line, and the dimension of each green port is indicated with an associated number.

A complementarity graph represents a "molecular program" to be executed physically by the corresponding DNA molecules. During the execution of the program through one-pot annealing (*25*), the specified complementarity relationship between the modular domains of the motif directs the DNA molecules toward a (global or local) thermodynamic minimum on the free energy landscape, where the designed target structure resides. For example, the execution of the molecular program in Fig. 1D results in the formation of the three-helix ribbon lattice depicted in Fig. 1B.

The three-helix ribbon program can be generalized to program the formation of *k*-helix ribbons (Fig. 2A), using $(k-1)$ full SST species (U_1, U_2, ..., U_{k-1}) and two boundary half-SST species (L_1 and L_k). By executing the general program in Fig. 2A, we demonstrate the experimental construction of monodisperse ribbons (*26*) with five distinct widths: 3-, 4-, 5-, 6-, and 20-helix ribbons. The secondary structure for the five-helix ribbon is depicted in Fig. 2B. Direct imaging of the self-assembly product by atomic force microscopy (AFM) reveals the expected linear filament morphology (Fig. 2C). AFM further confirms the designed dimensions of the ribbons: a *k*-helix ribbon has a measured width of ~3 × *k* nm (Fig. 2C insets). Further, the morphology details of the five-helix ribbon are revealed by high-resolution AFM (Fig. 2D).

A natural strategy for constructing monodisperse *k*-helix SST tubes is to merge the two boundary half-SST species in the *k*-helix ribbon program into a full SST species (Fig. 3A). The secondary structure for $k = 6$ is described in Fig. 3B (left). The execution of the six-helix tube program through annealing results in linear filament products (Fig. 4A, third panel from left). The mechanical force exerted by repeated AFM scanning opens these filaments, which confirms their tubular nature (fig. S12). Finally, AFM width measurement of 10 random opened tubes establishes the monodispersity (i.e., no $m \times 6$ -helix tubes identified, for $m > 1$) of their circumferences (fig. S13).

This molecular implementation could, in theory, allow concatenation of multiple repeats of U1-U2-U3-U4-U5-T6 along the tube's circumference, resulting in polydisperse tubes composed of 1 × 6 circumferential helices, 2 × 6 helices, 3 × 6 helices, etc. Further, geometric modeling (*12*) suggests that the SST domain dimensions in Fig. 3A would result in an average interhelix curvature of ~30° per helix (SOM text S1). One would, therefore, expect 12-helix tubes to be less sterically strained (*12*) than 6-helix tubes and, thus, to dominate at thermodynamic equilibrium. The observed monodisperse formation of six-helix tubes suggests that the tube formation should be understood as a kinetic process (*10*, *15*) and that these tubes are trapped at a local minimum on the free energy landscape (Fig. 3B, right). These tubes are stable: AFM images obtained ~6 months after sample preparation revealed monodisperse six-helix tubes.

We next tested the general program (Fig. 3A) where *k* distinct SST species self-assemble into *k*-helix tubes. By choosing appropriate subsets from a common pool of 15 distinct SST species (fig. S9), we have engineered monodisperse tubes of six different circumferences: 4-, 5-, 6-, 7-, 8-, and 10-helix tubes. The generality of this strategy is further confirmed by the successful engineering of monodisperse 20-helix tubes. The secondary structures of these tubes are presented in fig. S8. Their three-dimensional (3D) illustrations are

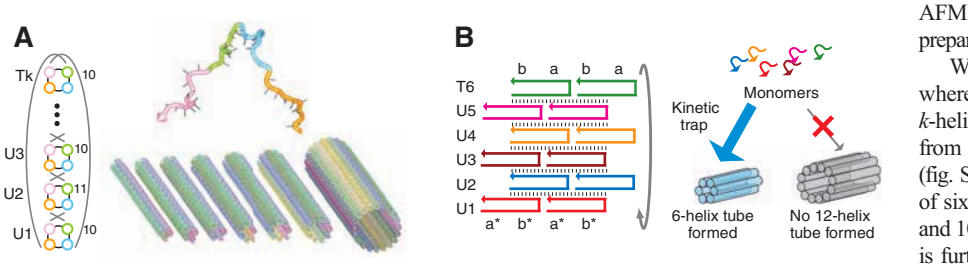

Fig. 3. Monodisperse DNA tubes with programmed circumferences. (**A**) Molecular program (left) and 3D illustrations (right) for assembling *k*-helix tubes. (**B**) Secondary structure (left) and putative kinetic trapping (right) for six-helix tubes. Asterisks denote complementarity.

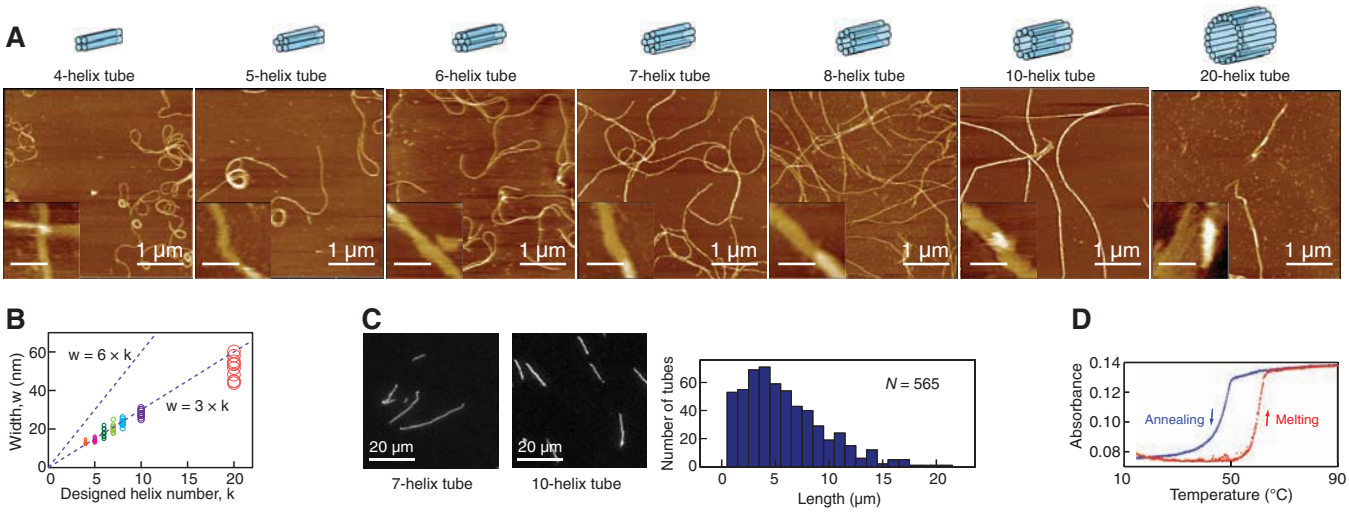

Fig. 4. (**A**) AFM images of 4-, 5-, 6-, 7-, 8-, 10-, and 20-helix tubes. See fig. S11 for larger AFM images. (Insets) Scale bar, 50 nm. (**B**) Width plot of opened tubes. A *k*-helix opened tube is expected to have a width $w \approx 3 \times k$ nm, as determined by the width measurement of the *k*-helix ribbons (fig. S6). A 2*k*-helix opened tube, in contrast, is expected to have $w \approx 6 \times k$ nm. Dashed lines corresponding to $w = 3 \times k$ and $w = 6 \times k$ are plotted to facilitate tube circumference monodispersity determination. See fig. S13 for a larger picture. (**C**) (Left) Fluorescence microscopy images of 7- and 10-helix tubes decorated with Cy3 fluorophores. (Right) Length profile of seven-helix tubes (sample size, $N = 565$). See fig. S14 for larger images and more profiles. (**D**) Annealing (blue) and melting (red) curves of four-helix tubes. Each constituent DNA strand at 100 nM. Cooling-heating rate at 0.15°C per minute. See fig. S15 for more thermal profiles.

Downloaded from www.sciencemag.org on August 7, 2008

summarized in Fig. 3A (right) and detailed in fig. S10. In each case, AFM imaging reveals the formation of long tubes (Fig. 4A), and AFM width measurement of randomly selected, opened tubes confirms the expected circumference monodispersity (Fig. 4A, insets, AFM images; Fig. 4B, a summary. See fig. S13 for details.) The length of SST tubes was investigated by using fluorescence microscopy (Fig. 4C). For seven-helix tubes, the average length is ~6 μm, with some tubes reaching ~20 μm.

Thermal formation and melting profiles of SST tubes (Fig. 4D) and SST ribbons (fig. S15) reveal hysteresis. Such hysteresis has also been observed in DNA lattices formed from multistranded tiles (*27*, *26*). It is also worth noting that the annealing and melting curves of SST tubes and ribbons demonstrate only one sharp transition temperature. This is consistent with the expectation that single-stranded DNA oligonucleotides are directly assembled into the growing lattice during annealing and disassembled from the lattice during melting. In contrast, two or more characteristic transition temperatures are commonly observed in lattices based on multistranded rigid tiles (*26*, *27*); the lowest temperature corresponds to lattice formation or melting, and the others correspond to tile formation or melting.

We suggest that the structural flexibility of SST may contribute to the success of the putative kinetic trapping of monodisperse tubes. The long sticky ends of SST and the flexible interhelix single-stranded linkage points in the assembled lattice may facilitate fast cyclization and hence trapping of the tubes with the smallest compatible number of helices. In addition, it is conceivable that in a nucleation-elongation model (*26*) (see fig. S16 for a hypothetical assembly pathway), the nucleation barrier difference between the *k*-helix tube and the 2*k*-helix tube may help trap the system into monodisperse *k*-helix tubes. The observed hysteresis (Fig. 4D) suggests the existence of a significant kinetic barrier during tube formation, and it is conceivable that this kinetic barrier is due to the presence of a nucleation barrier. It would be interesting to experimentally elucidate the kinetic assembly pathways of SST tubes. It would also be interesting to test if a similar kinetic strategy can be applied to programming the circumferences of DNA tubes assembled from multistranded rigid DNA tiles (*9*–*15*).

The ribbon and tube systems constructed here are likely to find applications ranging from biophysics to electronics and to nanotechnology. In biophysics, the programmable dimensions of the ribbons and tubes and, hence, their programmable physical properties, e.g., persistence length, make them attractive synthetic model systems. In electronics, metalization of DNA nanotubes (*9*, *11*, *17*) may result in nanowires with controlled diameters and, hence, controlled electronic properties. In nanotechnology, DNA nanotubes with programmable geometrical and mechanical properties can be used as building blocks for more sophisticated architectures and devices [e.g., tracks for molecular motors (*28*, *24*, *3*)] and as templates for organization of functional groups (*9*, *8*).

References and Notes

1. N. C. Seeman, *Nature* **421**, 427 (2003).
2. U. Feldkamp, C. M. Niemeyer, *Angew. Chem. Int. Ed.* **45**, 1856 (2006).
3. J. Bath, A. J. Turberfield, *Nat. Nanotechnol.* **2**, 275 (2007).
4. N. C. Seeman, *Mol. Biotechnol.* **37**, 246 (2007).
5. N. C. Seeman *et al.*, *Nanotechnology* **9**, 257 (1998).
6. T. J. Fu, N. C. Seeman, *Biochemistry* **32**, 3211 (1993).
7. E. Winfree, F. Liu, L. A. Wenzler, N. C. Seeman, *Nature* **394**, 539 (1998).
8. C. Lin, Y. Liu, S. Rinker, H. Yan, *ChemPhysChem* **7**, 1641 (2006).
9. H. Yan, S. H. Park, G. Finkelstein, J. H. Reif, T. H. LaBean, *Science* **301**, 1882 (2003).
10. J. C. Mitchell, J. R. Harris, J. Malo, J. Bath, A. J. Turberfield, *J. Am. Chem. Soc.* **126**, 16342 (2004).
11. D. Liu, S. H. Park, J. H. Reif, T. H. LaBean, *Proc. Natl. Acad. Sci. U.S.A.* **101**, 717 (2004).
12. P. W. K. Rothemund *et al.*, *J. Am. Chem. Soc.* **126**, 16344 (2004).
13. D. Reishus, B. Shaw, Y. Brun, N. Chelyapov, L. Adleman, *J. Am. Chem. Soc.* **127**, 17590 (2005).
14. H. Liu, Y. Chen, Y. He, A. E. Ribbe, C. Mao, *Angew. Chem. Int. Ed.* **45**, 1942 (2006).
15. Y. Ke, Y. Liu, J. Zhang, H. Yan, *J. Am. Chem. Soc.* **128**, 4414 (2006).
16. F. Mathieu *et al.*, *Nano Lett.* **5**, 661 (2005).
17. S. H. Park *et al.*, *Nano Lett.* **5**, 693 (2005).
18. B. Wei, Y. Mi, *Biomacromolecules* **6**, 2528 (2005).
19. W. B. Sherman, N. C. Seeman, *Biophys. J.* **90**, 4546 (2006).
20. S. M. Douglas, J. J. Chou, W. M. Shih, *Proc. Natl. Acad. Sci. U.S.A.* **104**, 6644 (2007).
21. A. Kuzuya, R. Wang, R. Sha, N. C. Seeman, *Nano Lett.* **7**, 1757 (2007).
22. The half-crossover can be viewed as a simplified Holliday-junction analog, which utilizes one strand, rather than the normal two strands, at the crossover exchange point. A similar structure was previously used in constructing DNA nanotubes (*14*).
23. Due to the modularity and standardization of the motif, assigning the dimensions of all the green domains in the lattice also uniquely determines the dimensions of all the other domains.
24. P. Yin, H. M. T. Choi, C. R. Calvert, N. A. Pierce, *Nature* **451**, 318 (2008).
25. Materials and methods are available as supporting material on *Science* Online.
26. R. Schulman, E. Winfree, *Proc. Natl. Acad. Sci. U.S.A.* **104**, 15236 (2007).
27. R. D. Barish, P. W. K. Rothemund, E. Winfree, *Nano Lett.* **5**, 2586 (2005).
28. R. Pei *et al.*, *J. Am. Chem. Soc.* **128**, 12693 (2006).

29. The authors thank E. Winfree at Caltech for generously hosting the majority part of this work in his lab. For inspiring discussions, the authors thank E. Winfree, P. W. K. Rothemund, R. Schulman, V. A. Beck, J. R. Vieregg, R. D. Barish, B. Yurke, D. Y. Zhang, N. A. Pierce, S. Hamada, M. Bockrath, H. Maune, Y. Huang, C. R. Calvert, N. L. Dabby, and J. Kim. The authors are also grateful to N. A. Pierce at Caltech and J. Liu at Duke for facility support, to the Pierce group for the use of the unpublished DNA sequence design component and DNA structure illustration component of the NUPACK server (www.nupack.org), and to B. Walters for technical assistance. The fluorescence microscope was built by R.F.H. and B. Yurke. There is a patent pending on this work. This work is supported by the Center for Biological Circuit Design at Caltech, NSF grants CCF-0523555 and CCF-0432038 to J.H.R., NSF grant CBET-0508284 to T.H.L., NSF grants 0622254 and 0432193 to E. Winfree, and NSF grant 0506468 to N. A. Pierce.

Supporting Online Material

www.sciencemag.org/cgi/content/full/321/5890/824/DC1
Materials and Methods
Texts S1 and S2
Figs. S1 to S16

4 March 2008; accepted 16 June 2008
10.1126/science.1157312

The Role of Excited-State Topology in Three-Body Dissociation of *sym*-Triazine

John D. Savee,[1] Vadim A. Mozhayskiy,[2] Jennifer E. Mann,[1] Anna I. Krylov,[2]* Robert E. Continetti[1]*

Molecular fragmentation into three products poses an analytical challenge to theory and experiment alike. We used translational spectroscopy and high-level ab initio calculations to explore the highly debated three-body dissociation of *sym*-triazine to three hydrogen cyanide molecules. Dissociation was induced by charge exchange between the *sym*-triazine radical cation and cesium. Calculated state energies and electronic couplings suggest that reduction initially produces a population of *sym*-triazine partitioned between the 3s Rydberg and $\pi^* \leftarrow n$ electronically excited manifolds. Analysis of the topology of these manifolds, along with momentum correlation in the dissociation products, suggests that a conical intersection of two potential energy surfaces in the 3s Rydberg manifold leads to stepwise dissociation, whereas a four-fold glancing intersection in the $\pi^* \leftarrow n$ manifold leads to a symmetric concerted reaction.

Molecular dissociation plays an important role in the chemistry of nonequilibrium environments where sufficient energy is available to break a chemical bond. Most photoinitiated dissociation processes in the lower layers of Earth's atmosphere are two-body processes, for which dynamical information can be obtained through relatively straightforward experiments. However, in combustion processes, the stratosphere, interstellar space, and other lower-density environments, high-energy processes (e.g., dissociative recombination) can read-

Downloaded from www.sciencemag.org on August 7, 2008